SUPPLEMENTARY INFORMATION

Boron-based Pd_3B_{26} alloy cluster as a nanoscale antifriction bearing system: tubular core-shell structure, double π/σ aromaticity, and dynamic structural fluxionality

Lin-Yan Feng,[a,b] Jin-Chang Guo,[a] Ying-Jin Wang,[b] Xiao-Ying Zhang,[a] and Hua-Jin Zhai*[a]

[a]*Nanocluster Laboratory, Institute of Molecular Science, Shanxi University, Taiyuan 030006, China*

[b]*Department of Chemistry, Xinzhou Teachers University, Xinzhou 034000, China*

*E-mail: hj.zhai@sxu.edu.cn

Supplementary Information – Part I

Table S1. Cartesian coordinates for key structures of the alloy Pd_3B_{26} cluster system at the PBE0/def2-TZVP level. Cluster **1** (C_s, $^1A'$) is the most stable structure as identified from our global structure searches in this work. Structure **2** (C_s, $^1A'$) represents a transition state (TS), which is relevant to dynamic structural fluxionality of the system.

Figure S1. Alternative optimized low-lying structures of Pd_3B_{26} cluster at the PBE0/def2-TZVP level, along with their relative energies (in eV). Also shown in the square brackets are the relative energies at the B3LYP/def2-TZVP level. The comparative energetics data serve to check for computational consistency of the

density-functional theory (DFT) methods. All energies listed have the corrections for zero-point energies (ZPEs).

Figure S2. Optimized geometric structures of (a) cluster **1** (C_s, $^1A'$) and (b) TS structure **2** (C_s, $^1A'$) of Pd_3B_{26} cluster at the PBE0/def2-TZVP level. Calculated bond distances are labelled in Å (black color; top panels), for which the B–B value represents the average B–B distance within the B_{13} rings. The Wiberg bond indices (WBIs; in blue color) and natural atomic charges (in |e|, red color) are obtained from the natural bond orbital (NBO) analyses, also at the PBE0/def2-TZVP level.

Figure S3. Pictures of selected canonical molecular orbitals (CMOs) for Pd_3B_{26} **1** (C_s, $^1A'$) cluster. These CMOs are associated to the quasi-Lewis-type three-center two-electron (3c-2e) B–B σ bonds along two peripheral B_{13} rings, showing a certain extent of σ bonding between two B_{13} rings.

Figure S4. An alternative AdNDP scheme for Pd_3B_{26} **1** (C_s, $^1A'$) cluster. Herein the skeleton B–B σ bonding is strictly partitioned as Lewis-type 2c-2e σ single bonds along two B_{13} rings with relatively low occupation numbers (ONs) of 1.77–1.82 |e|, which is not in line with the CMO data as described in Section 4.1. Therefore, this AdNDP scheme has fundamental flaws. Our preferred AdNDP bonding scheme is presented in Figure 4.

Figure S5. Pictures of selected CMOs for TS Pd_3B_{26} **2 (**C_s, $^1A'$) structure. These CMOs are also associated to peripheral quasi-Lewis-type 3c-2e σ bonds, similar to those in Figure S3.

Figure S6. Occupied CMOs of TS **2** structure of Pd_3B_{26} cluster. These CMOs are similar to those in Figure 2, except for a slightly spatial shift in the orientation of electron clouds.

Figure S7. The AdNDP bonding scheme of TS **2** structure of Pd_3B_{26} cluster. ONs are indicated.

Supplementary Information – Part II

A short movie extracted from the BOMD simulation for Pd_3B_{26} cluster. The simulation was performed at 300 K for 50 ps. The movie roughly covers a time span of 25 ps.

Table S1. Cartesian coordinates for key structures of the alloy Pd_3B_{26} cluster system at the PBE0/def2-TZVP level. Cluster **1** (C_s, $^1A'$) is the most stable structure as identified from our global structure searches in this work. Structure **2** (C_s, $^1A'$) represents a transition state (TS), which is relevant to dynamic structural fluxionality of the system.

(a) Pd_3B_{26} (**1**, C_s, $^1A'$)

B	0.78406900	3.02918800	1.47240900
B	0.78406900	3.02918800	-1.47240900
B	0.78112300	0.26377700	-3.18235600
B	0.74632400	-2.60519500	-2.40523400
B	0.74632400	-2.60519500	2.40523400
B	0.78112300	0.26377700	3.18235600
B	0.74054800	-1.33558900	-3.40869900
B	0.78727000	1.65737300	-2.34374300
B	0.76107500	3.69435600	0.00000000
B	0.78727000	1.65737300	2.34374300
B	0.74054800	-1.33558900	3.40869900
B	-0.78583800	-0.47542200	3.40919900
B	-0.79306000	-2.89285400	1.60899200
B	-0.79279000	-2.03094600	-2.97300100
B	-0.76608600	1.06887200	-2.92874500
B	-0.76735200	3.46181600	-0.80973300
B	-0.76458800	2.44672000	2.06635500
B	-0.76458800	2.44672000	-2.06635500
B	-0.78583800	-0.47542200	-3.40919900
B	-0.79306000	-2.89285400	-1.60899200
B	-0.79279000	-2.03094600	2.97300100

B	-0.76608600	1.06887200	2.92874500
B	-0.76735200	3.46181600	0.80973300
B	0.77169800	-2.90874200	-0.81400700
B	0.77169800	-2.90874200	0.81400700
B	-0.78171900	-3.07803400	0.00000000
Pd	-0.01909600	1.49720100	0.00000000
Pd	0.01704800	-0.74720500	-1.29334400
Pd	0.01704800	-0.74720500	1.29334400

(b) TS, Pd_3B_{26} (**2**, C_s, $^1A'$)

B	3.60574500	0.79644800	0.00000000
B	3.02085100	0.79328100	-1.50436100
B	1.77025700	0.77609500	-2.53157800
B	0.31002700	0.78042200	-3.23865000
B	-1.30100400	0.77931000	-3.34084700
B	-2.58975000	0.77363100	-2.36265200
B	-3.04975800	0.76076600	-0.81332600
B	-3.04975800	0.76076600	0.81332600
B	-2.58975000	0.77363100	2.36265200
B	-1.30100400	0.77931000	3.34084700
B	0.31002700	0.78042200	3.23865000
B	1.77025700	0.77609500	2.53157800
B	3.02085100	0.79328100	1.50436100
B	3.51943900	-0.73893500	0.80920200
B	3.51943900	-0.73893500	-0.80920200
B	2.39771300	-0.77414200	-1.97422700
B	0.97920300	-0.77870500	-2.77153700
B	-0.50556300	-0.76511700	-3.42613600

B	-2.07776100	-0.75193000	-3.04671200
B	-2.84627700	-0.78688100	-1.62647100
B	-2.84296200	-0.78937400	0.00000000
B	-2.84627700	-0.78688100	1.62647100
B	-2.07776100	-0.75193000	3.04671200
B	-0.50556300	-0.76511700	3.42613600
B	0.97920300	-0.77870500	2.77153700
B	2.39771300	-0.77414200	1.97422700
Pd	1.49217100	-0.02480000	0.00000000
Pd	-0.74703900	0.00464600	-1.29633900
Pd	-0.74703900	0.00464600	1.29633900

Figure S1. Alternative optimized low-lying structures of Pd_3B_{26} cluster at the PBE0/def2-TZVP level, along with their relative energies (in eV). Also shown in the square brackets are the relative energies at the B3LYP/def2-TZVP level. The comparative energetics data serve to check for computational consistency of the density-functional theory (DFT) methods. All energies listed have the corrections for zero-point energies (ZPEs). Selected triplet structures that correspond to the low-lying singlets are also optimized (not shown), and the lowest-energy triplet state cluster has a relative energy of 0.27 eV at PBE0.

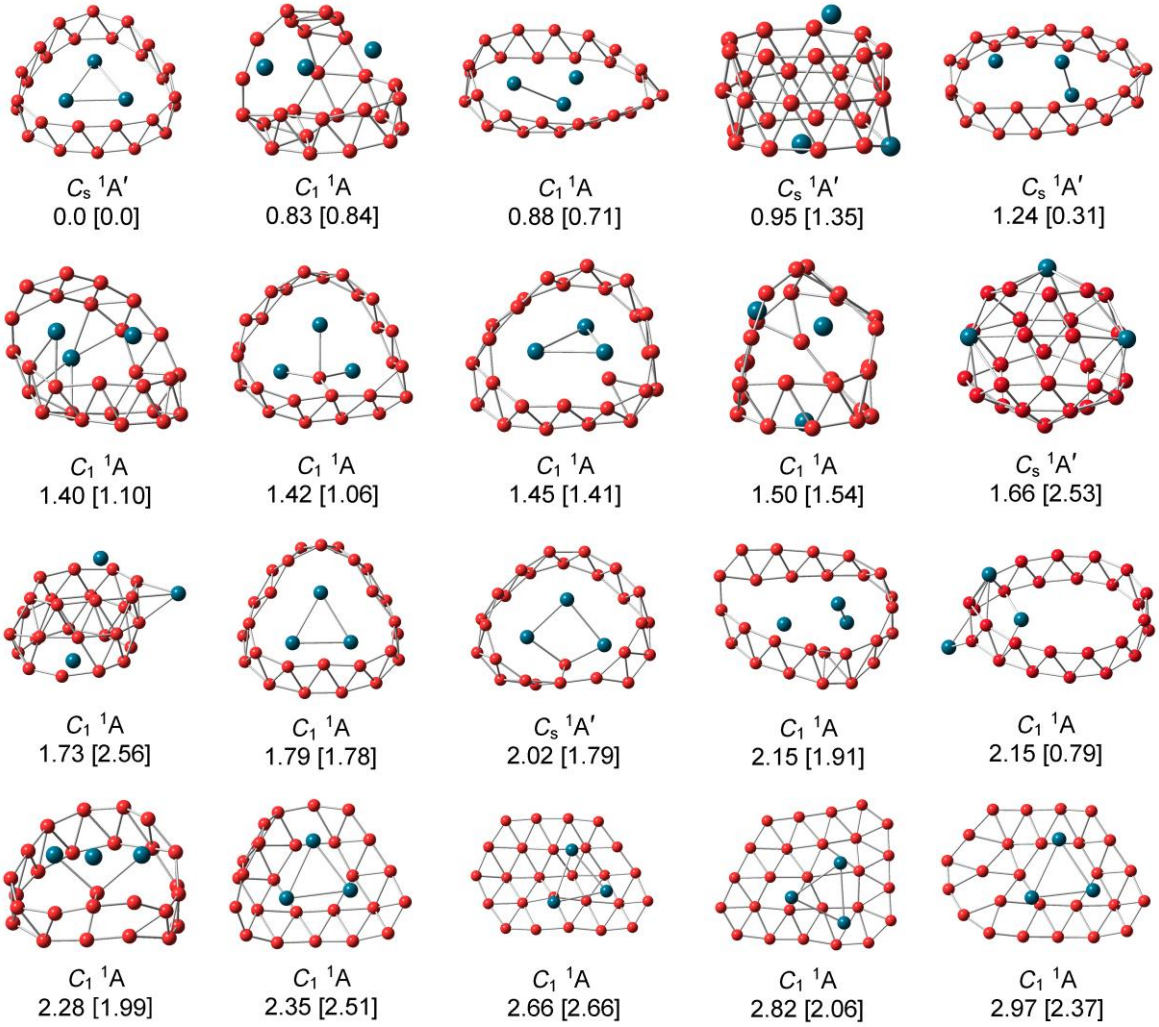

Figure S2. Optimized geometric structures of (a) cluster **1** (C_s, ^{1}A′) and (b) TS structure **2** (C_s, ^{1}A′) of Pd_3B_{26} cluster at the PBE0/def2-TZVP level. Calculated bond distances are labelled in Å (black color; top panels), for which the B–B value represents the average B–B distance within the B_{13} rings. The Wiberg bond indices (WBIs; in blue color) and natural atomic charges (in |e|, red color) are obtained from the natural bond orbital (NBO) analyses, also at the PBE0/def2-TZVP level.

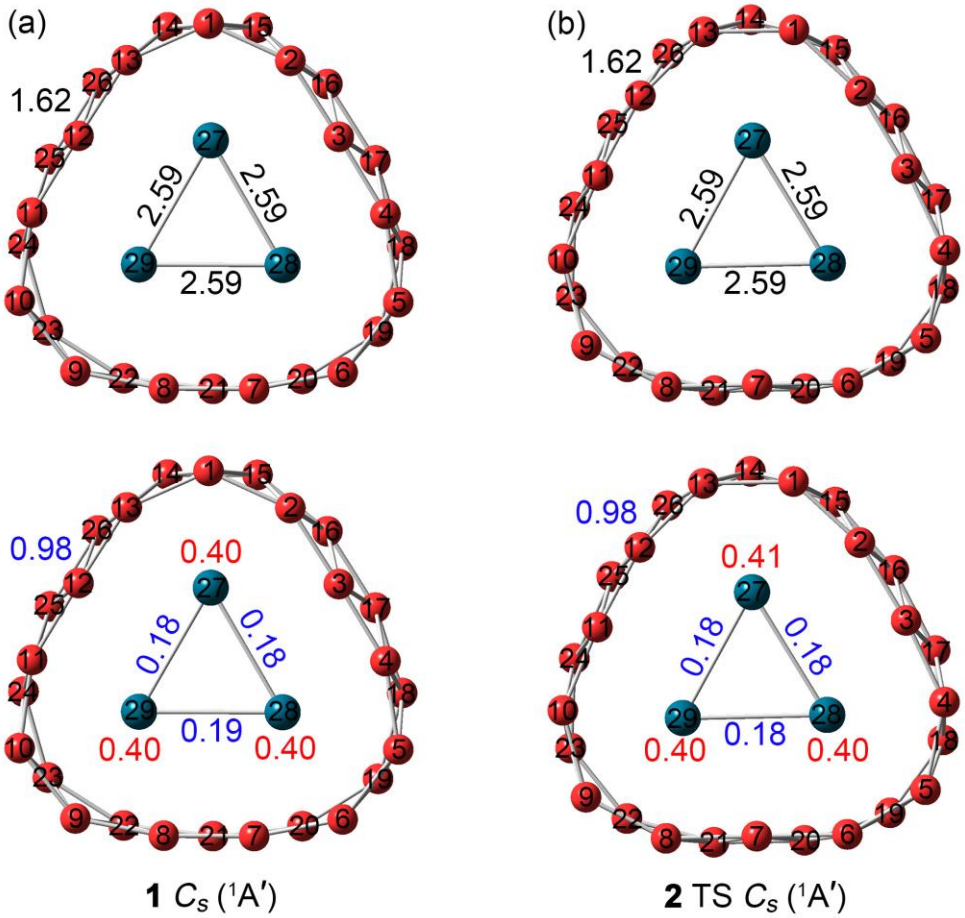

Figure S3. Pictures of selected canonical molecular orbitals (CMOs) for Pd_3B_{26} **1** (C_s, $^1A'$) cluster. These CMOs are associated to the quasi-Lewis-type three-center two-electron (3c-2e) B–B σ bonds along two peripheral B_{13} rings, showing a certain extent of σ bonding between two B_{13} rings.

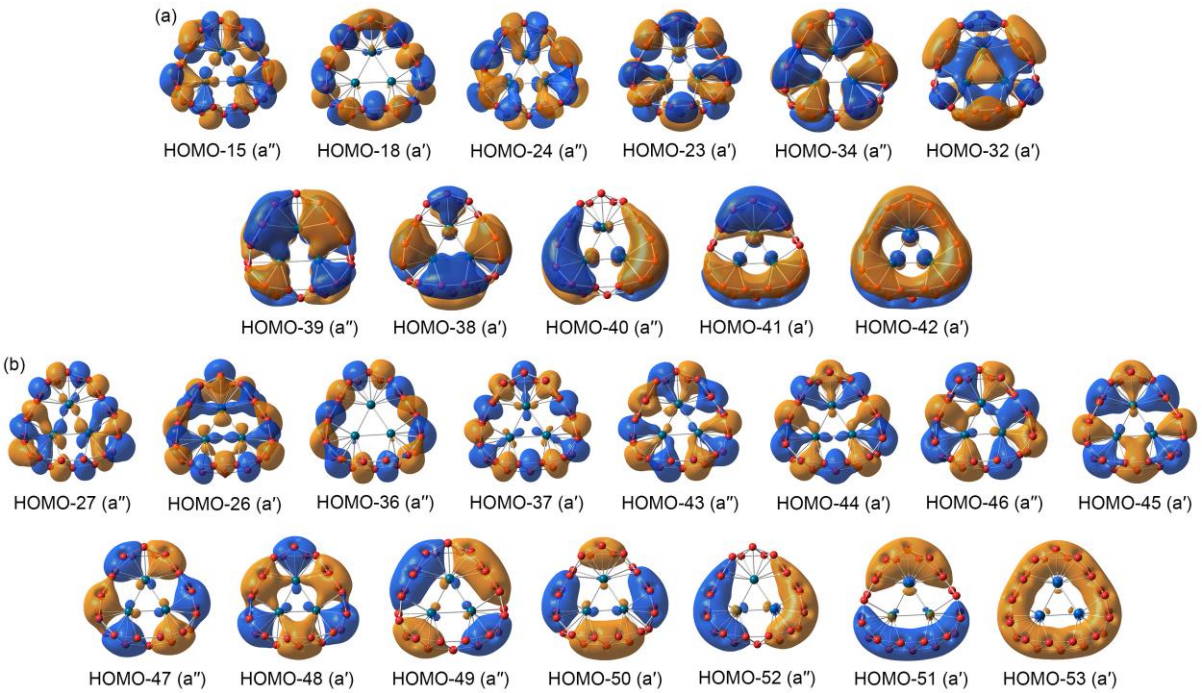

Figure S4. An alternative AdNDP scheme for Pd_3B_{26} **1** (C_s, $^1A'$) cluster. Herein the skeleton B–B σ bonding is strictly partitioned as Lewis-type 2c-2e σ single bonds along two B_{13} rings with relatively low occupation numbers (ONs) of 1.77–1.82 |e|, which is not in line with the CMO data as described in Section 4.1. Therefore, this AdNDP scheme has fundamental flaws. Our preferred AdNDP bonding scheme is presented in Figure 4.

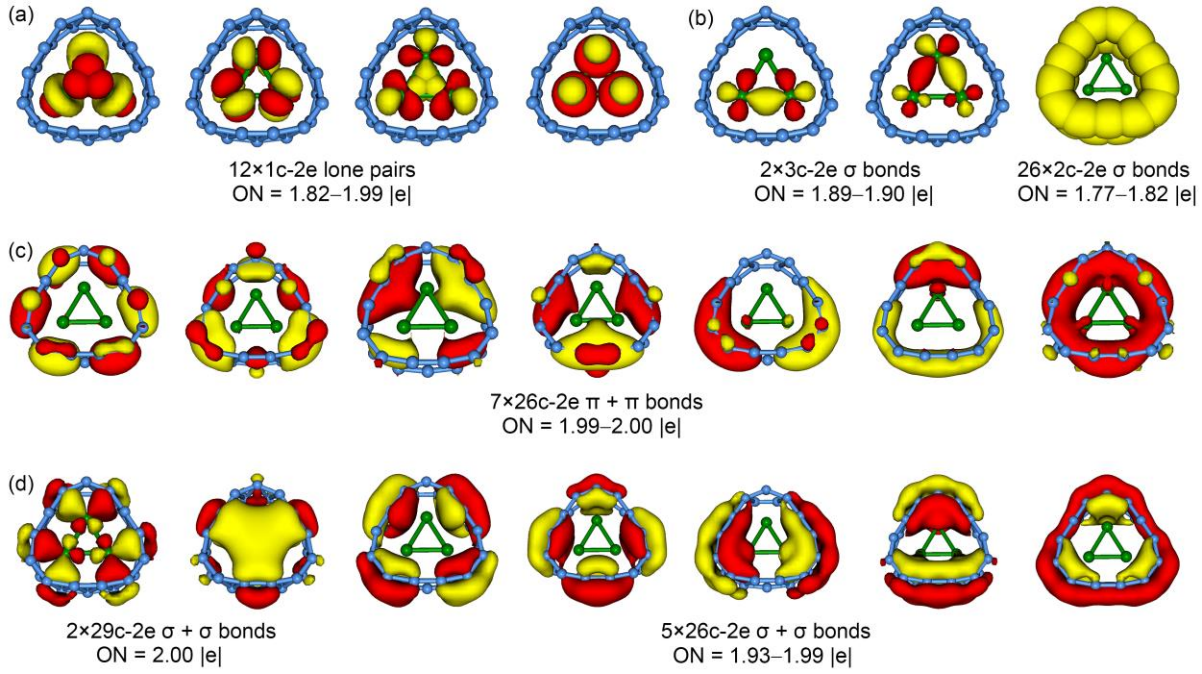

Figure S5. Pictures of selected CMOs for TS Pd_3B_{26} **2** (*C*$_s$, ^{1}A′) structure. These CMOs are also associated to peripheral quasi-Lewis-type 3c-2e σ bonds, similar to those in Figure S3.

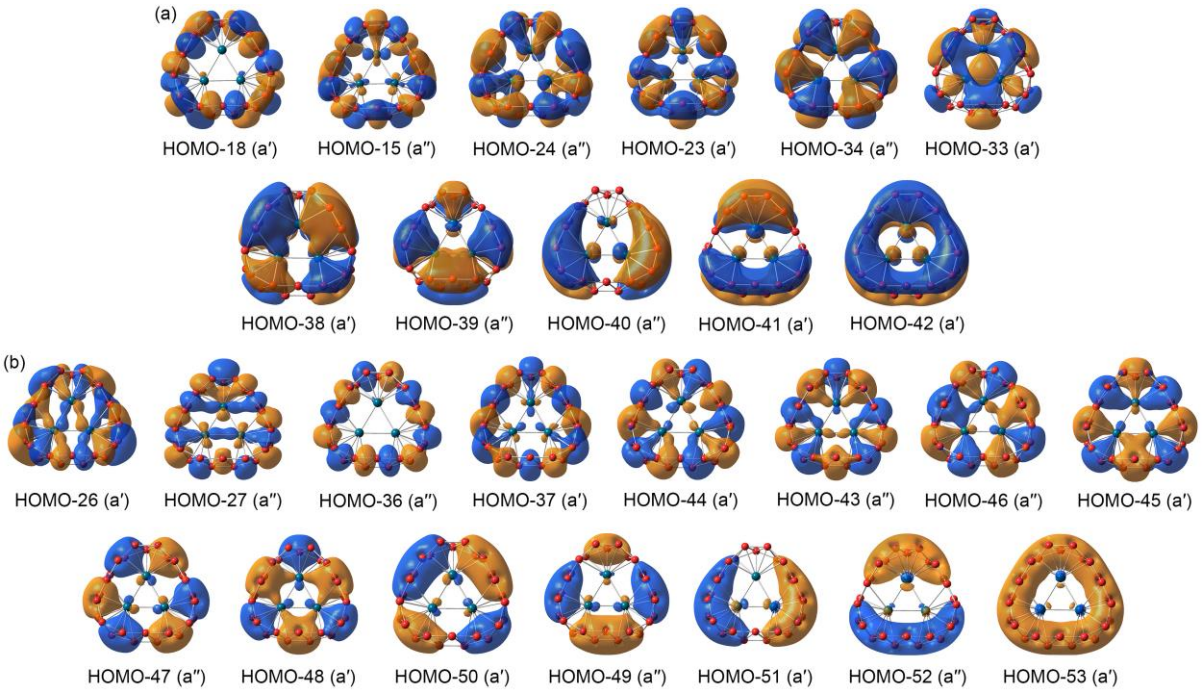

Figure S6. Occupied CMOs of TS **2** structure of Pd_3B_{26} cluster. These CMOs are similar to those in Figure 2, except for a slightly spatial shift in the orientation of electron clouds.

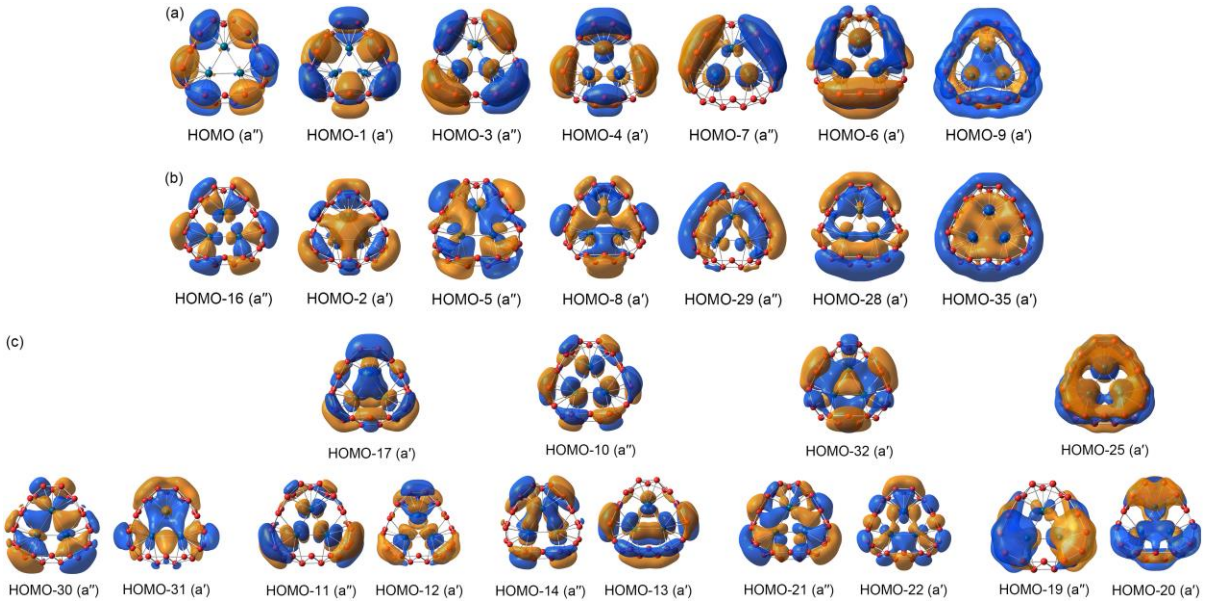

Figure S7. The AdNDP bonding scheme of TS **2** structure of Pd_3B_{26} cluster. ONs are indicated.